Supplement of Atmos. Chem. Phys., 21, 14893–14906, 2021
https://doi.org/10.5194/acp-21-14893-2021-supplement

Atmospheric Chemistry and Physics
Open Access
EGU

Supplement of

Characterization of non-refractory (NR) PM_1 and source apportionment of organic aerosol in Kraków, Poland

Anna K. Tobler et al.

Correspondence to: Andre S. H. Prevot (andre.prevot@psi.ch)

S1 Quality control of NR-PM_1 ACSM measurements

The ACSM was routinely calibrated with NH_4NO_3 and $(NH_4)_2SO_4$ to determine the RF_{NO_3}, RIE_{NH4} and RIE_{SO4} in full scan mode, meaning that the same scanning protocol was used during the calibration as during ambient measurements (Freney et al., 2019). In addition, the ACSM was also calibrated with NH_4Cl to determine the RIE_Chl', following the procedure described by Tobler et al. (2020), where the RIE_Chl' is only based on the ion signals of frag_HCl and does not include frag_Cl. An average RF_{NO3} = 4.68 ± 1.66×10−11 A (µg m^{-3})$^{-1}$ was applied together with an RIE_{NH4} = 2.43 ± 0.58, RIE_{SO4} = 0.38 ± 0.11 RIE_Chl′ =0.41 ± 0.17.

Unfortunately, co-located total $PM_{2.5}$ measurements were not available at AGH University for quality control. However, total $PM_{2.5}$ reference data was available from the monitoring station ("Bujaka station") run by the Chief Inspectorate for Environmental Protection, located ca. 6.8 km south-east of the AGH monitoring station. Taking into account that the two stations are 6.8 km apart and in a urban area, which means that local sources could be contributing quite differently, there is still a decent correlation of R^2 = 0.67 and a reasonable slope of 0.77.

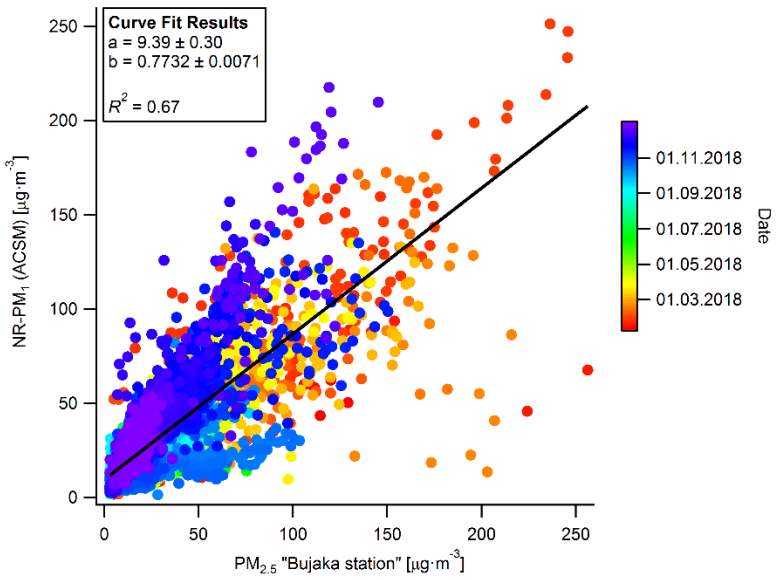

Figure S1. NR-PM_1 measured by the ACSM at AGH University versus total $PM_{2.5}$ measured at the Bujaka station.

S2 Quality control of Aethalometer eBC measurements

The eBC mass concentration measured with Aethalometers was calibrated as the relationship between the optical measurement of light attenuation (ATN) and the thermal measurement of carbonaceous mass on filters extracted of non-refractive material (Gundel et al., 1984). The slope of this relationship is the mass attenuation cross-section. Gundel et al. (1984) used urban samples for their calibration. The ratio between the mass attenuation cross-section and MAC is the multiple scattering enhancement parameter C, the multiplication parameter describing the light absorption enhancement due to the light scattering filter matrix in which the particles are embedded (Drinovec et al., 2015). The eBC measurement is cross-sensitive to scattering (Drinovec et al., 2015) with the susceptibility depending on the filter type and the sample (Yus-Díez et al., 2021). These site-dependent artifacts are explicitly observed as the changes in the slope between different filter photometers in regional background sites, featuring high single-scattering albedo (Yus-Díez et al., 2021; Zanatta et al., 2016).

The continuity of calibration of Aethalometers was ensured with comparisons at urban sites with low single-scattering albedo and fresh aerosol (Drinovec et al., 2015; Gundel et al., 1984). The measurement artifacts related to high single-scattering albedo, internal mixing of aged BC and cross-sensitivity to scattering are not prevalent in urban atmospheres (Yus et al., 2021) and therefore we do not expect them to be relevant for our studies in Krakow. The eBC mass concentration should be linearly dependent on the time derivative of ATN, there should be no dependence on ATN itself – any dependence is the manifestation of the loading non-linearities of the measurement that is the saturation of the measurement and the associated decrease of measurement the sensitivity.

In Fig. S2 we see the BC(ATN) plot determined from the data for the whole measurement campaign from January 2018 to April 2019, for the wavelengths used in the source apportionment algorithm (Sandradewi et al., 2008): 470 nm and 950 nm. The slope, remaining after the internal correction by the Aethalometer (Drinovec et al., 2015), is minimal with the artifact below 5% for the case of 950 nm channel and even less for the 470 nm channel.

The maximum ATN at which the measurements are restarted on a new piece of tape (tape is advanced) is set for UV as ATN_{max} (370 nm) =120. This translates to ATN_{max} (950 nm) = 46, assuming BC is the only component of the sample and this parameter changes inversely with wavelength – this is the same assumption as taking absorption Angstrom exponent AAE=1. The real value at 950 nm depends on the real sample absorption at this wavelength of interest, therefore on the wavelength dependence of absorption and hence AAE. So, the value at 950 nm is lower than what one would expect by assuming AAE=1 and extrapolating from 370nm. Additionally, high concentrations with very loaded filter (high ATN) trigger the advance of tape and start of the measurement with a fresh tape (ATN = 0). To void the bias due to these very high concentrations, we have determined the slope in the interval between ATN=2 and ATN = 0.85 ATN_{max} for each wavelength of interest.

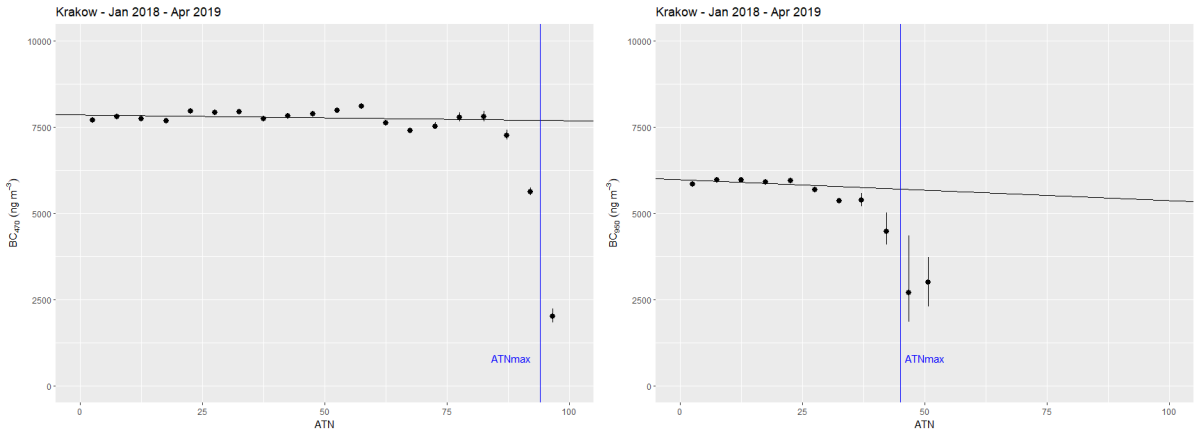

Figure S2. BC(ATN) plots for the measurements at 470 nm (left) and 950 nm (right). The negligible slope demonstrates an absence of loading effects.

Source apportionment uses source specific values of the Ångström exponent (AAE). The traffic features the AAE value between 0.9 and 1.1. The value for solid fuel is less well determined as it depends on the efficiency of combustion. These source specific values are supposed to be representative for the source, but are in fact a single value representing the center of a distribution for this particular source. In the absence of validation measurements (for example C14, (Zotter et al., 2017)), plotting the probability density function can serve as a guide for the determination of these values as seen in Fig. S3. Source specific values for traffic AAE_{tr} = 0.85 and solid fuel AAE_{sf}= 1.9 were selected. We see in Fig. S3 the AAE probability density function (PDF) for all Krakow Aethalometer absorption data calculated in two different ways. First, the AAE was calculated as the ratio of the logarithms of the absorption coefficient:

$$AAE = \frac{\ln(b_{370}/b_{950})}{\ln(950/370)}$$

and it is shown in blue in Figure 3. The AAE obtained from the fit of the absorption coefficient as a function of the wavelength (from 370 nm to 950 nm) is shown in green with applying a very stringent filter r^2>0.99 for the fit. The resulting PDF (in green) substantially shrinks the tails of the PDF compared to the PDF of the AAE as a ratio. This filtering allows only the "best" fits and the end PDF values are the ones that we can ascribe to two sources - the tails for this stringent-filtered data end at the values that we chose for the source specific AAE values.

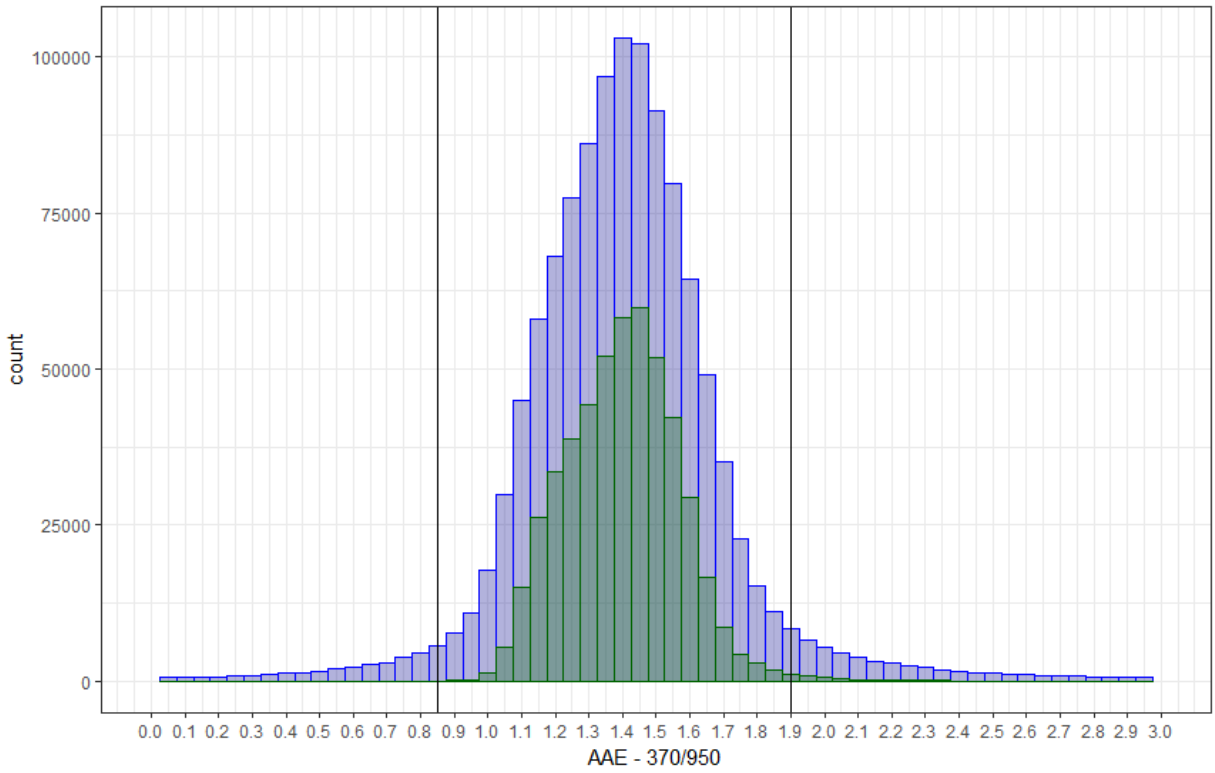

Figure S3. The absorption Ångström exponent (AAE) probability density function: AAE calculated from the ratio of the 370 nm and 950 nm channels (blue) and from the fit off all wavelengths from 370 nm to 950 nm and filtered for fit r^2>0.99.

S3 Supplementary NR-PM$_1$ material

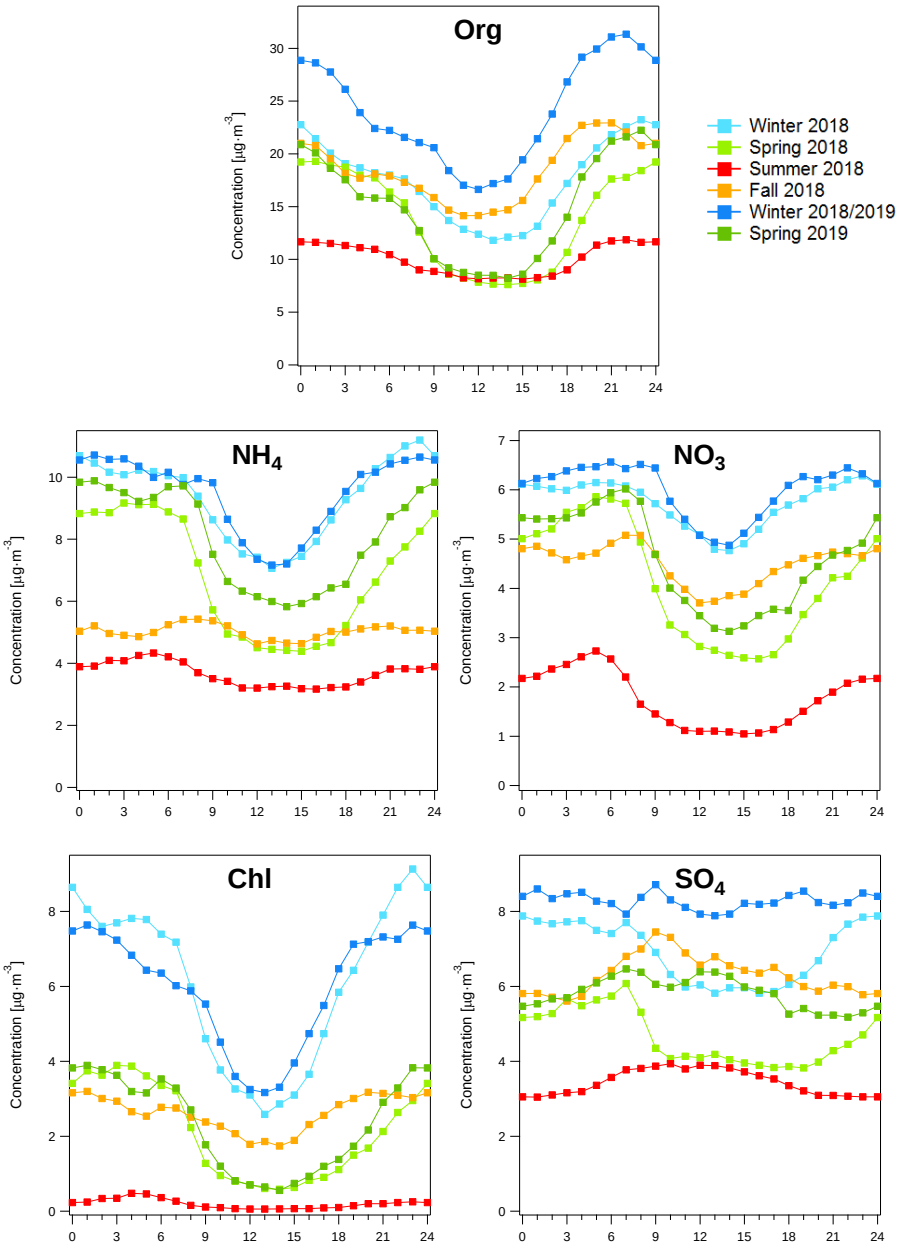

Figure S4. Seasonal diurnal cycles of the ACSM species color-coded by season.

S4 Rolling PMF settings

After evaluation of the seasonal PMF solutions, rolling PMF was performed. The rolling PMF approach is defined by the shift parameter (amount of days by which the PMF window is shifted), the width of the PMF window (amount of consecutive days over which PMF is performed) and the number of repeats per PMF window. The PMF window was always shifted by 1 day in this study to capture variations of the emission sources best (Canonaco et al., 2021). For this study window lengths of 7, 14, 21 and 28 days were tested. The same set of criteria and thresholds was used on all four different PMF analyses to better compare them. Previously, the number of non-modelled days was used to determine the optimum window length (Canonaco et al., 2021). For a window length of 7 days, 4.2 % of the time points were not modelled. In all the other tested window lengths (14, 21 and 27 days), all data points were modelled. The PMF errors slightly decreased with longer window length, although not significantly. While a shorter window is favorable since unique time periods (i.e., special pollution events) will be less propagated into the PMF results, the window should still be long enough to capture systematical changes and filter out short-term fluctuations. Therefore, the 14-day window length solution was chosen here.

The repeats per window are required for the study of the statistical uncertainties of the rolling PMF approach. On the one hand, the statistical uncertainty can be assessed by the application of the bootstrap technique, where the PMF input is randomly resampled before each PMF initialization. If factors are constrained with *a priori* information (reference profiles or external time series), the rotational ambiguity has to be explored by a sensitivity analysis of the *a*-value. It has been shown by Canonaco et al. (2021) that the exploration of the solution space with the full *a*-value range (0 to 1) is not necessary unless high *a*-values were already required for the seasonal pretests. Furthermore, the random exploration of the possible *a*-value combinations (in contrast to explicitly checking every possible *a*-value combination) has proven sufficient. For this study, the *a*-values were chosen randomly for each PMF repetition, as well as independently for each factor, ranging for 0 to an upper *a*-value of 0.4 for HOA, BBOA and CCOA ($\Delta a = 0.1$). The upper cut-off was determined based on the seasonal pretests as for solutions with higher *a*-values the POAs were subject to mixing of profiles.

8193 solutions (36.9 %) out of the total 22’200 single PMF runs generated during the rolling PMF approach were regarded as environmentally reasonable based on the criteria described above. All time points were modelled. Analysis of the scaled residuals over time and variables (*m/z*) did not reveal any systematic errors, as shown in Fig. S5. The rolling PMF in combination with the bootstrap resampling strategy and the random *a*-value approach for the constrained factors, results in the repeated sampling of each time point *i*. The statistical and rotational uncertainty is represented by the variability among the time points *i*. The uncertainty is described as the logarithmic probability density function (pdf) of the standard deviation of each time point *i* divided by the mean concentration of each time point *i*. As time points with a low signal-to-noise ratio would pull the error calculations, the lognormal distribution was chosen to better represent the PMF errors.

As shown in Fig. S7, the relative PMF errors are ± 27.1 %, ± 26.1 %, ± 14.6 %, ± 21.8 % and ± 39.2 % for HOA, BBOA, CCOA, MO-OOA and LO-OOA, respectively.

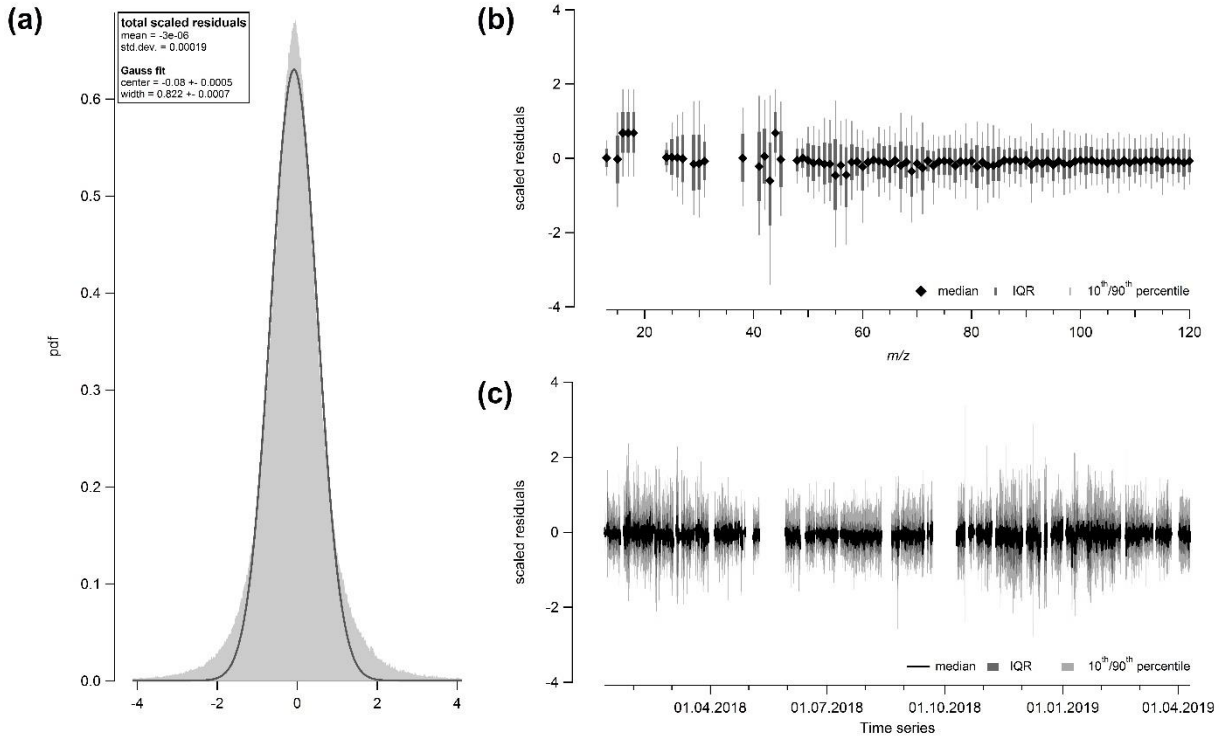

Figure S5. Analysis of the scaled residuals shows no systematic over- or underestimation for (a) the total scaled residuals, (b) the scaled residuals over the *m/z*'s and (c) the scaled residuals over time.

S5 Supplementary PMF results

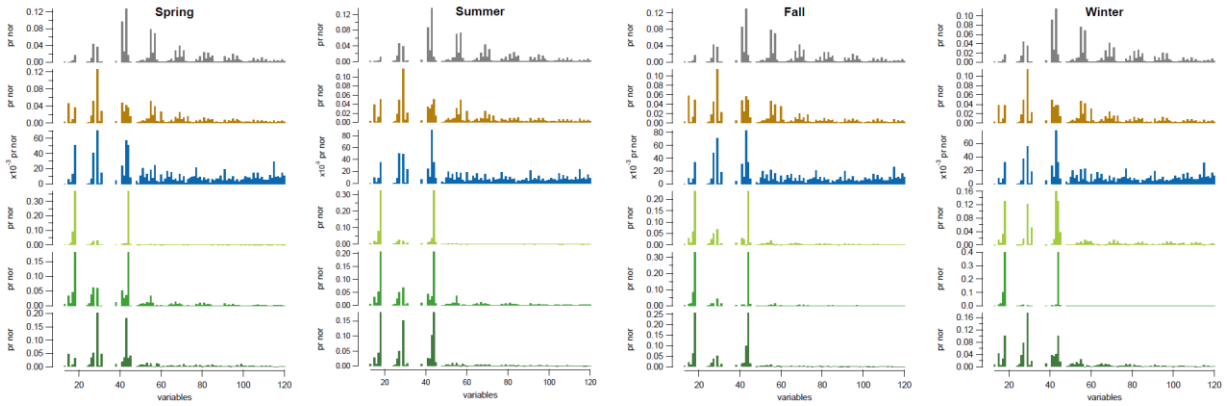

Figure S6. Rejected 6-factor solution based on seasonal PMF. Based on the mass spectral profile as well as the diurnal evolution, it appears that the OOA is splitting into three factors.

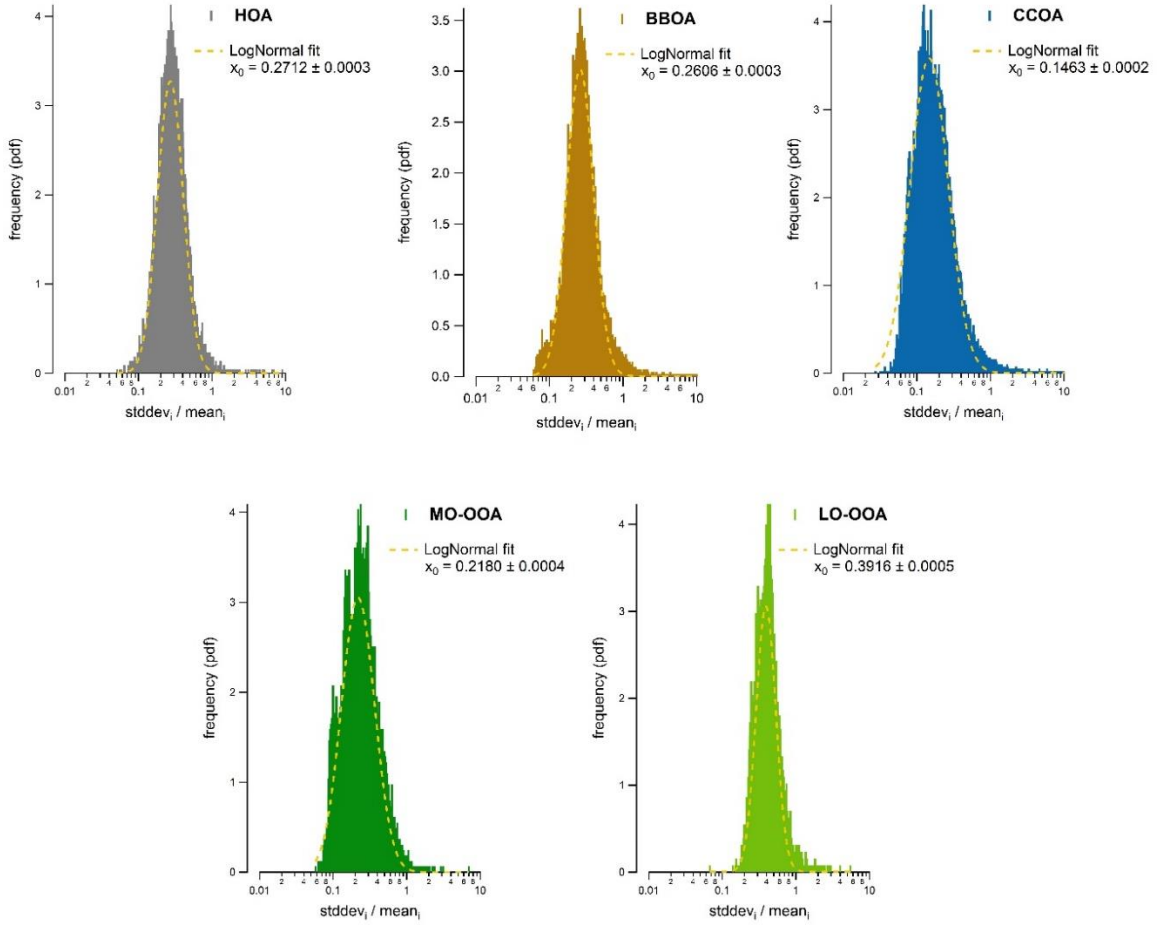

Figure S7. PMF error estimation of the five resolved PMF factors represented as logarithmic probability density functions (pdf) of the standard deviations of each time point *i* divided by the mean concentration of each time point *i*.

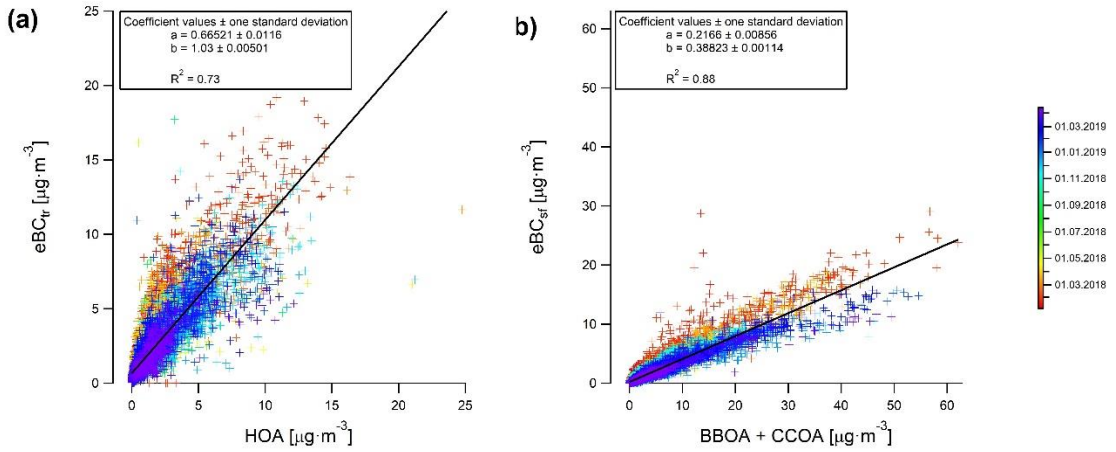

Figure S8. (a) eBC_{tr} versus HOA and (b) eBC_{sf} vs (BBOA + CCOA).

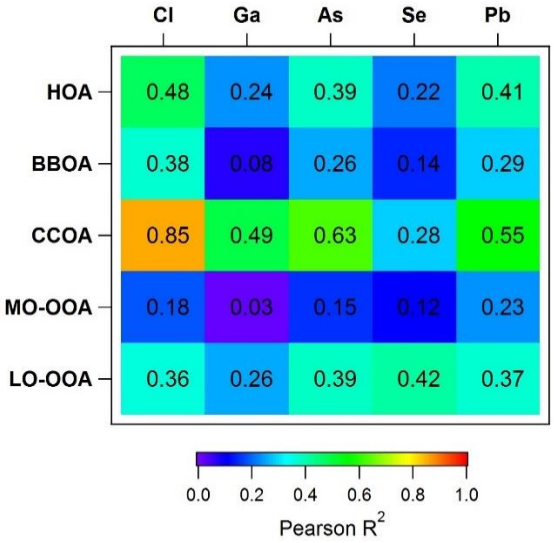

Figure S9. Correlation (Pearson R^2) of the coal-related elements measured by the Xact and all OA factors.

Table S1. Average seasonal OA to eBC ratios.

	2018				2019	
Season	Winter	Spring	Summer	Fall	Winter	Spring
Average OA/eBC (± standard deviation)	2.67 ± 1.03	4.43 ± 2.35	8.22 ± 3.57	5.74 ± 2.33	5.78 ± 2.28	6.01 ± 2.51

References

Canonaco, F., Tobler, A., Chen, G., Sosedova, Y., Slowik, J. G., Bozzetti, C., Daellenbach, K. R., El Haddad, I., Crippa, M., Huang, R.-J., Furger, M., Baltensperger, U., and Prévôt, A. S. H.: A new method for long-term source apportionment with time-dependent factor profiles and uncertainty assessment using SoFi Pro: application to 1 year of organic aerosol data, Atmos. Meas. Tech., 14, 923-943, https://doi.org/10.5194/amt-14-923-2021, 2021.

Drinovec, L., Mocnik, G., Zotter, P., Prevot, A. S. H., Ruckstuhl, C., Coz, E., Rupakheti, M., Sciare, J., Muller, T., Wiedensohler, A., and Hansen, A. D. A.: The "dual-spot" Aethalometer: an improved measurement of aerosol black carbon with real-time loading compensation, Atmos. Meas. Tech., 8, 1965-1979, https://doi.org/10.5194/amt-8-1965-2015, 2015.

Freney, E., Zhang, Y. J., Croteau, P., Amodeo, T., Williams, L., Truong, F., Petit, J. E., Sciare, J., Sarda-Esteve, R., Bonnaire, N., Arumae, T., Aurela, M., Bougiatioti, A., Mihalopoulos, N., Coz, E., Artinano, B., Crenn, V., Elste, T., Heikkinen, L., Poulain, L., Wiedensohler, A., Herrmann, H., Priestman, M., Alastuey, A., Stavroulas, I., Tobler, A., Vasilescu, J., Zanca, N., Canagaratna, M., Carbone, C., Flentje, H., Green, D., Maasikmets, M., Marmureanu, L., Minguillon, M. C., Prevot, A. S. H., Gros, V., Jayne, J., and Favez, O.: The second ACTRIS inter-comparison (2016) for Aerosol Chemical Speciation Monitors (ACSM): Calibration protocols and instrument performance evaluations, Aerosol Sci. Technol., https://doi.org/10.1080/02786826.2019.1608901, 2019.

Gundel, L. A., Dod, R. L., Rosen, H., and Novakov, T.: The relationship between optical attenuation and black carbon concentration for ambient and source particles, Sci. Total Environ., 36, 197-202, https://doi.org/10.1016/0048-9697(84)90266-3, 1984.

Sandradewi, J., Prevot, A. S. H., Szidat, S., Perron, N., Alfarra, M. R., Lanz, V. A., Weingartner, E., and Baltensperger, U.: Using Aerosol Light Absorption Measurements for the Quantitative Determination of Wood Burning and Traffic Emission Contributions to Particulate Matter, Environ. Sci. Technol., 42, 3316-3323, https://doi.org/10.1021/es702253m, 2008.

Tobler, A. K., Skiba, A., Wang, D. S., Croteau, P., Styszko, K., Nęcki, J., Baltensperger, U., Slowik, J. G., and Prévôt, A. S. H.: Improved chloride quantification in quadrupole aerosol chemical speciation monitors (Q-ACSMs), Atmos. Meas. Tech., 13, 5293-5301, https://doi.org/10.5194/amt-13-5293-2020, 2020.

Yus-Díez, J., Bernardoni, V., Močnik, G., Alastuey, A., Ciniglia, D., Ivančič, M., Querol, X., Perez, N., Reche, C., Rigler, M., Vecchi, R., Valentini, S., and Pandolfi, M.: Determination of the multiple-scattering correction factor and its cross-sensitivity to scattering and wavelength dependence for different AE33 Aethalometer filter tapes: A multi-instrumental approach, Atmos. Meas. Tech. Discuss., 2021, 1-30, https://doi.org/10.5194/amt-2021-46, 2021.

Zanatta, M., Gysel, M., Bukowiecki, N., Müller, T., Weingartner, E., Areskoug, H., Fiebig, M., Yttri, K. E., Mihalopoulos, N., Kouvarakis, G., Beddows, D., Harrison, R. M., Cavalli, F., Putaud, J. P., Spindler, G., Wiedensohler, A., Alastuey, A., Pandolfi, M., Sellegri, K., Swietlicki, E., Jaffrezo, J. L., Baltensperger, U., and Laj, P.: A European aerosol phenomenology-5: Climatology of black carbon optical properties at 9 regional background sites across Europe, Atmos. Environ., 145, 346-364, https://doi.org/10.1016/j.atmosenv.2016.09.035, 2016.

Zotter, P., Herich, H., Gysel, M., El-Haddad, I., Zhang, Y. L., Mocnik, G., Huglin, C., Baltensperger, U., Szidat, S., and Prevot, A. H.: Evaluation of the absorption Angstrom exponents for traffic and wood burning in the Aethalometer-based source apportionment using radiocarbon measurements of ambient aerosol, Atmos. Chem. Phys., 17, 4229-4249, https://doi.org/10.5194/acp-17-4229-2017, 2017.